Draft version January 13, 2016
Preprint typeset using LaTeX style emulateapj v. 5/2/11

arXiv:1510.04288v3 [astro-ph.HE] 12 Jan 2016

NEUTRON-STAR MERGER EJECTA AS OBSTACLES TO NEUTRINO-POWERED JETS OF GAMMA-RAY BURSTS

O. Just[1,2], M. Obergaulinger[3], H.-T. Janka[1], A. Bauswein[4,5], and N. Schwarz[1,6]

Draft version January 13, 2016

ABSTRACT

We present the first special relativistic, axisymmetric hydrodynamic simulations of black hole-torus systems (approximating general relativistic gravity) as remnants of binary-neutron star (NS-NS) and neutron star-black hole (NS-BH) mergers, in which the viscously driven evolution of the accretion torus is followed with self-consistent energy-dependent neutrino transport and the interaction with the cloud of dynamical ejecta expelled during the NS-NS merging is taken into account. The modeled torus masses, BH masses and spins, and the ejecta masses, velocities, and spatial distributions are adopted from relativistic merger simulations. We find that energy deposition by neutrino annihilation can accelerate outflows with initially high Lorentz factors along polar low-density funnels, but only in mergers with extremely low baryon pollution in the polar regions. NS-BH mergers, where polar mass ejection during the merging phase is absent, provide sufficiently baryon-poor environments to enable neutrino-powered, ultrarelativistic jets with terminal Lorentz factors above 100 and considerable dynamical collimation, favoring short gamma-ray bursts (sGRBs), although their typical energies and durations might be too small to explain the majority of events. In the case of NS-NS mergers, however, neutrino emission of the accreting and viscously spreading torus is too short and too weak to yield enough energy for the outflows to break out from the surrounding ejecta shell as highly relativistic jets. We conclude that neutrino annihilation alone cannot power sGRBs from NS-NS mergers.

Subject headings: gamma-ray burst: general — neutrinos — accretion, accretion disks — hydrodynamics

1. INTRODUCTION

Binary neutron star (NS-NS) and neutron star-black hole (NS-BH) mergers release huge amounts of energy in a short time and a small spatial volume. Therefore, a possible role of these events as sources of cosmic gamma-ray bursts has been proposed already decades ago (Paczynski 1986; Eichler et al. 1989). Well localized short gamma-ray bursts (sGRBs) provide observational support for such a connection in particular because of their low-density environments, partially large offsets from their galactic hosts and their occurrence also in galaxies with low star-formation activity (Nakar 2007; Berger 2014; Fong et al. 2015).

NS-NS and NS-BH mergers can produce BH-torus systems as remnants, or in the former case also massive neutron stars (MNSs), which could be transiently or long-term stable, depending on their mass and the uncertain nuclear equation of state (EOS). The GRB is understood as consequence of highly collimated, ultrarelativistic polar outflows or jets of low-density plasma or Poynting flux, whose energy is partly converted to γ-rays at distances of 10^{12}–10^{13} cm, far away from the compact remnant (e.g. Piran 2004). As possible energy sources to drive these jets, the annihilation of neutrino-antineutrino pairs radiated by the hot accretion torus is discussed (e.g. Eichler et al. 1989; Woosley 1993; Jaroszynski 1993; Ruffert & Janka 1999; Popham et al. 1999; Di Matteo et al. 2002; Birkl et al. 2007, Dessart et al. 2009, Zalamea & Beloborodov 2011) or the energy release by magnetohydrodynamic effects, Poynting flux (e.g. Blandford & Znajek 1977; McKinney & Blandford 2009; Paschalidis et al. 2015) or electron-positron pair production (Usov 1992) associated with ultrastrong magnetic fields threading the BH-torus system or MNS and their environments.

Individual aspects and special questions of these scenarios have been intensively investigated previously, for example the emergence of a jet-favorable magnetic field configuration in NS-NS/BH mergers (Paschalidis et al. 2015; Kiuchi et al. 2015; Dionysopoulou et al. 2015), the efficiency of neutrino production in accretion disks and tori with steady-state accretion rate (e.g. Popham et al. 1999; Di Matteo et al. 2002; Chen & Beloborodov 2007), the efficiency of neutrino-antineutrino ($\nu\bar{\nu}$-) annihilation above the poles of a BH (e.g. Birkl et al. 2007; Zalamea & Beloborodov 2011; Richers et al. 2015), or the jet acceleration and collimation by the interaction with the accretion torus, non-relativistic winds (Aloy et al. 2005; Murguia-Berthier et al. 2014) or the ejecta from dynamical NS-NS mergers (Nagakura et al. 2014; Duffell et al. 2015). Also, time-dependent and self-consistent hydrodynamic simulations of BH-torus remnants including some neutrino treatment have been performed to study neutrino emission and annihilation (Ruffert & Janka 1999; Setiawan et al. 2004, 2006; Fernández & Metzger 2013; Just et al. 2015a; Foucart et al. 2015).

In this work we focus on the neutrino-powered GRB scenario. For the first time, we simulate (in axisymmetry) the evolution of BH-torus systems including (magnetic-field related) viscosity effects, energy-dependent neutrino transport and $\nu\bar{\nu}$-annihilation. Moreover, we include self-consistently the formation of relativistic polar outflows and their interaction with the rapidly expanding, subrelativistic ejecta shell that is dynamically expelled during binary NS merging. The

ojust@mpa-garching.mpg.de, thj@mpa-garching.mpg.de
[1] Max-Planck-Institut für Astrophysik, Karl-Schwarzschild-Str. 1, 85748 Garching, Germany
[2] Max-Planck/Princeton Center for Plasma Physics (MPPC)
[3] Departament d´Astronomia i Astrofísica, Universitat de València, Edifici d´Investigació Jeroni Muñoz, C/ Dr. Moliner, 50, E-46100 Burjassot (València), Spain
[4] Department of Physics, Aristotle University of Thessaloniki, 54124 Thessaloniki, Greece
[5] Heidelberger Institut für Theoretische Studien, Schloss-Wolfsbrunnenweg 35, 69118 Heidelberg, Germany
[6] Physik Department, Technische Universität München, James-Franck-Straße 1, 85748 Garching, Germany

TABLE 1
MODEL PROPERTIES AND RESULTS

Name	M_1/M_2	$M_{\rm BH}$	$A_{\rm BH}$	$m_{\rm torus}$	$\alpha_{\rm vis}$	$m_{\rm env}$	$m_{\rm env,pol}$	$\bar{v}_{\rm env}$	$\bar{v}_{\rm env,pol}$	$E^{\rm pol}_{\rm ann}$	$E^{\rm iso}_{\rm ann}$	$\bar{\eta}_\nu$	$\bar{\eta}_{\rm ann}$	$T_{\rm NDAF}$	$T^{90}_{\rm ann}$	$E_{\Gamma>10/100}$	$\theta_{\Gamma>10/100}$	$E^{\rm iso}_{\Gamma>10/100}$
	$[M_\odot]$	$[M_\odot]$		$[M_\odot]$		$[10^{-3}M_\odot]$	$[m_{\rm dyn}]$	[c]	[c]	$[10^{49}$ erg]	$[10^{49}$ erg]	[%]	[%]	[ms]	[ms]	$[10^{48}$ erg]	[°]	$[10^{50}$ erg]
SFHO_145145	1.45/1.45	2.77	0.78	0.11	0.06	16	31 %	0.12	0.14	1.19	4.06	2.3	0.23	204	27	0/0	0/0	0/0
SFHO_1218	1.2/1.8	2.78	0.76	0.14	0.06	3.5	16 %	0.42	0.68	1.60	5.46	2.4	0.26	238	29	0/0	0/0	0/0
SFHO_1218a3	1.2/1.8	2.78	0.76	0.14	0.03	3.5	16 %	0.42	0.68	0.91	3.11	2.9	0.12	565	47	0/0	0/0	0/0
SFHO_1218a12	1.2/1.8	2.78	0.76	0.14	0.12	3.5	16 %	0.42	0.68	2.31	7.89	1.9	0.47	93	19	0/0	0/0	0/0
TM1_13520	1.35/2.0	3.09	0.75	0.19	0.06	18	5.8 %	0.21	0.40	2.16	7.37	2.3	0.26	283	34	0/0	0/0	0/0
TM1_1451	1.4/5.1	6.08	0.83	0.34	0.06	–	–	–	–	1.38	4.71	2.4	0.10	392	72	8.17/2.05	34/8.2	0.48/2.0

NOTE. — Each model name indicates the nuclear EOS used in the merger simulation, i.e. TM1 (Hempel et al. 2012) or SFHO (Steiner et al. 2013). Values of time-dependent quantities are given at the final simulation times. The sub-/superscript 'pol' indicates quantities within the two polar cones of half-opening angle 45°. All quantities are defined in the main text.

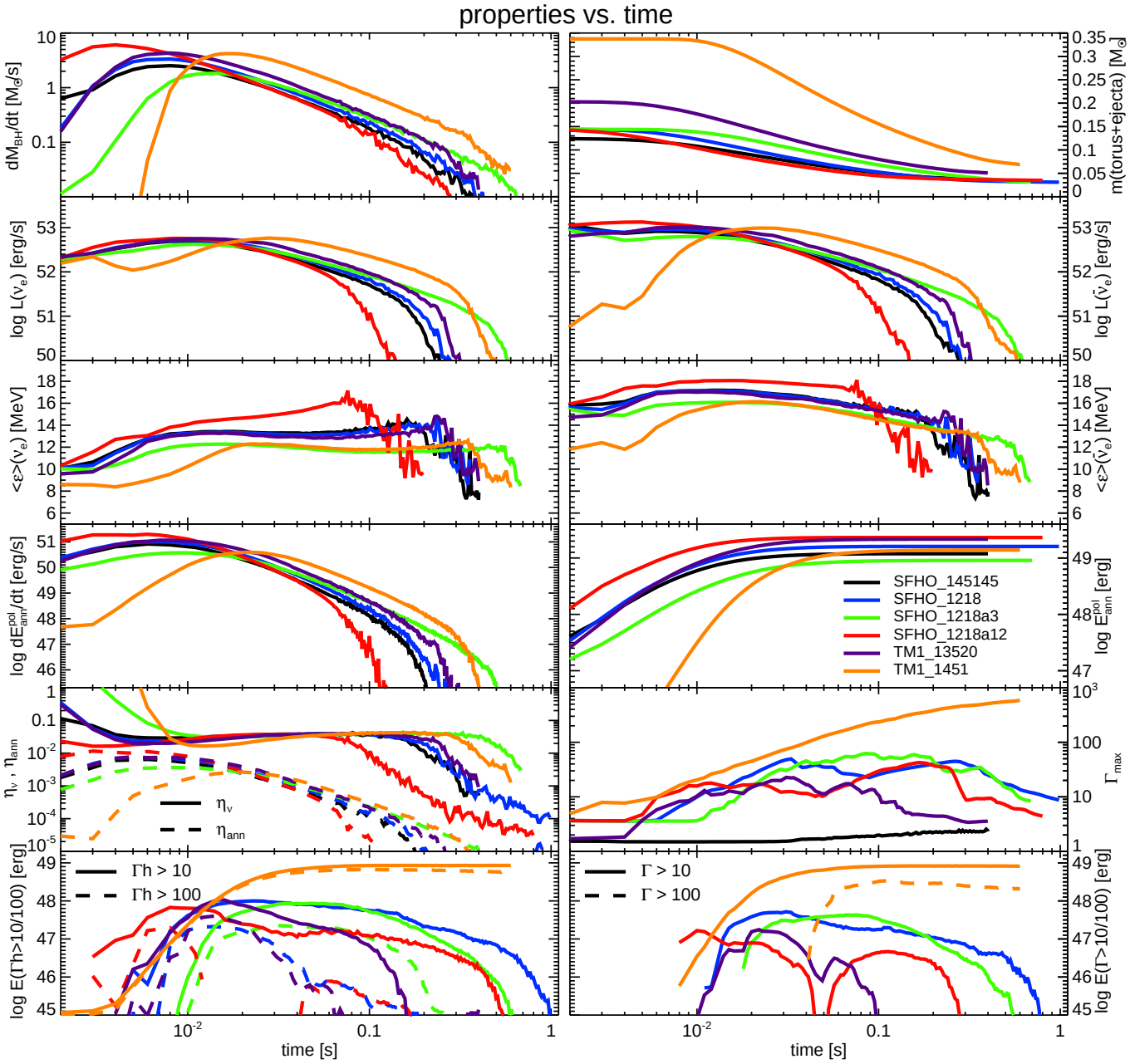

FIG. 1.— Time evolution of the mass-accretion rate, $\dot{M}_{\rm BH}$, torus plus ejecta mass, m, electron neutrino and antineutrino luminosities, $L_{\nu_e,\bar{\nu}_e}$, mean energies $\langle\varepsilon\rangle_{\nu_e,\bar{\nu}_e}$, total annihilation rate, $\dot{E}^{\rm pol}_{\rm ann}$, deposited annihilation energy, $E^{\rm pol}_{\rm ann}$, efficiencies of neutrino emission, η_ν, and annihilation, $\eta_{\rm ann}$, maximum Lorentz factor, $\Gamma_{\rm max}$, and total energies carried by material with Γh or Γ above 10 or 100, $E_{\Gamma h>10/100}$ and $E_{\Gamma>10/100}$, respectively. The mean energies are defined as $\langle\varepsilon\rangle_\nu \equiv L_\nu/L_{N,\nu}$, where $L_{N,\nu}$ is the total number emission rate, and L_ν, $L_{N,\nu}$ are measured in the lab-frame at $r = 500$ km.

considered ejecta and remnant conditions (masses, spins, expansion velocities, energies) are set up in accordance with relativistic NS-NS and NS-BH merger simulations. The goal of our study is to investigate the requirements for neutrino-powered GRB jets.

2. NUMERICAL TREATMENT AND MODEL SETUP

The simulations were performed with the ALCAR code (Just et al. 2015b) that solves the equations of hydrodynamics along with a multi-energy group M1-type scheme for the neutrino transport. Most input physics is adopted from BH-torus simulations presented in Just et al. (2015a). However, we now use a special relativistic instead of a Newtonian solver for the Euler equations, allowing us to accurately follow relativistic jet outflows. Note that in the bulk of the disk the conditions are at most mildly relativistic, hence the torus evolution and the properties of the subrelativistic ejecta as described in Just et al. (2015b) remain essentially unaffected by switching to the relativistic solver. For the same reason we keep using the Newtonian version of the viscosity terms.

The transport of electron neutrinos and antineutrinos employs 10 energy groups distributed logarithmically within $[0, 80\,\mathrm{MeV}]$ and source terms for absorption, emission and scattering interactions with free nucleons (as given in Bruenn 1985). The velocities entering the neutrino transport are subject to the restrictions explained in Just et al. (2015a). Energy- and momentum-transfer rates due to $\nu\bar{\nu}$-annihilation are calculated from the annihilation-rate 4-vector (Birkl et al. 2007, typos corrected by Zalamea & Beloborodov 2011) expressed in terms of the evolved neutrino moments (analogously to Eq. 10 of Dessart et al. 2009) and are used as source terms for the hydrodynamic equations. Since we are only interested in the effects of annihilation near the baryon-poor funnel, we ignore annihilation in regions where the density $\rho > 10^{11}\,\mathrm{g\,cm^{-3}}$ or where neutrino cooling dominates heating.

We apply a microphysical equation of state (including a 4-species baryon gas, electrons, positrons and photons), the pseudo-Newtonian gravitational potential by Artemova et al. (1996), and a viscosity scheme using $\alpha_{\rm vis}$ to parametrize magnetohydrodynamic, turbulent angular momentum transport (Shakura & Sunyaev 1973; in the version denoted as "type 2" in Just et al. 2015a). The initial torus equilibrium configuration is computed as described in Just et al. (2015a) for given initial mass, $M_{\rm BH}$, and dimensionless spin parameter, $A_{\rm BH}$, of the BH, and torus mass, $m_{\rm torus}$ (see Just et al. 2015a and references therein for details). For these quantities we adopt values guided by merger simulations that were performed (and partially discussed in Just et al. 2015a) with a relativistic smoothed-particle hydrodynamics (SPH) code using the conformal flatness condition (Oechslin et al. 2002; Bauswein 2010).

To take into account the envelope of material – mostly containing dynamical ejecta – around the BH-torus system formed during the merger, we map the azimuthally averaged distributions of density, electron fraction, pressure, and velocity from the corresponding original merger model onto the grid regions surrounding our manually constructed torus. We utilize the SPH configurations resulting at about ∼1–5 ms after the BH formation and identify the isotropic coordinate radius with our radial coordinate r (see Bauswein et al. 2013, for details concerning the dynamical ejecta). However, we disregard all material from the merger model for radii $r < 50\,\mathrm{km}$ because, first, the inconsistency between both radius versions grows for smaller radii, and second, because the original SPH torus is replaced by our self-constructed torus. The remaining volume surrounding the torus and envelope is initially filled with a dynamically irrelevant amount of cold gas having a density of $\rho = 1.5\,\mathrm{g\,cm^{-3}}$ for $r \le 10^3$ km and $\propto r^{-4}$ for higher radii.

We assume equatorial and axi-symmetry and use spherical polar coordinates. However, although we simulate only one hemisphere we always take into account both hemispheres for volume integration. The radial grid consists of 800 zones of exponentially increasing width and extends from ∼(1–2)×10^6 cm up to ∼3×10^{11} cm. The angular grid consists of 120 zones linearly distributed within the domain $[0°, 30°]$ and another 120 zones of exponentially increasing width covering $[30°, 90°]$. We validated numerical convergence of our main results.

We consider three NS-NS merger models (Table 1). Model SFHO_145145 is characterized by symmetric progenitor masses, M_1, M_2, and a delayed (∼10 ms) BH formation after the merger, while models SFHO_1218 and TM1_13520 result from asymmetric mergers and prompt BH formation. Hence (Bauswein et al. 2013), compared to the former model both latter models exhibit a lower total envelope mass, $m_{\rm env}$, and a reduced fraction of mass, $m_{\rm env,pol}/m_{\rm env}$, located in the two polar cones with 45° half-opening angle ($m_{\rm env,pol}/m_{\rm env} \approx 0.29$ would result for an isotropic distribution), while the corresponding average velocities, $\bar{v}_{\rm env}$, $\bar{v}_{\rm env,pol}$, are higher (Table 1). Two models with different values of $\alpha_{\rm vis}$ are added to investigate the dependence on viscosity. For model TM1_1451 linked to a NS-BH merger (Table 1) we do not map any material from the merger simulation onto our grid, because in NS-BH mergers the dynamical ejecta are almost exclusively expelled in the equatorial direction (e.g. Just et al. 2015a) and therefore have a strongly reduced impact on the jet compared to NS-NS mergers.

To assess the efficiency of $\nu\bar{\nu}$-annihilation for most optimistic cases, we employ favorable rather than typical merger configurations (except for SFHO_145145, e.g. Dominik et al. 2012; Lattimer 2012), slightly overestimated torus masses (e.g. Kyutoku et al. 2015), and a neutrino treatment that tends to overestimate the $\nu\bar{\nu}$-annihilation rates near the poles (see the comparison of M1 with ray-tracing results in Just et al. 2015a).

3. RESULTS

3.1. *Torus evolution, neutrino emission and annihilation*

The time evolution of several quantities characterizing the $\nu\bar{\nu}$-annihilation is illustrated in Fig. 1. All modeled tori traverse the two evolutionary phases denoted as NDAF and ADAF (neutrino- and advection-dominated accretion flow, respectively; see e.g., Metzger et al. 2008; Fernández & Metzger 2013; Just et al. 2015a). In the NDAF phase the temperatures and thus neutrino production rates are high enough for viscous heating to be efficiently compensated by neutrino emission, while in the subsequent ADAF phase neutrino reactions cease and ultimately freeze out owing to low temperatures. During the NDAF phase torus mass accreted onto the BH per unit of time, $\dot{M}_{\rm BH}$, is converted into energy-emission rates (i.e. luminosities) of both neutrino species, $L_{\nu_e,\bar{\nu}_e}$, with an efficiency $\eta_\nu \equiv (L_{\nu_e} + L_{\bar{\nu}_e})/(\dot{M}_{\rm BH}c^2)$ (with the speed of light c) of a few per cent (Fig. 1). After being emitted, a fraction of neutrinos pair-annihilate, giving rise to a local heating rate, $Q_{\rm ann}$ (Figs. 2– 4), which is highest close to the BH, since here the neutrino densities are largest, and steeply decreases with

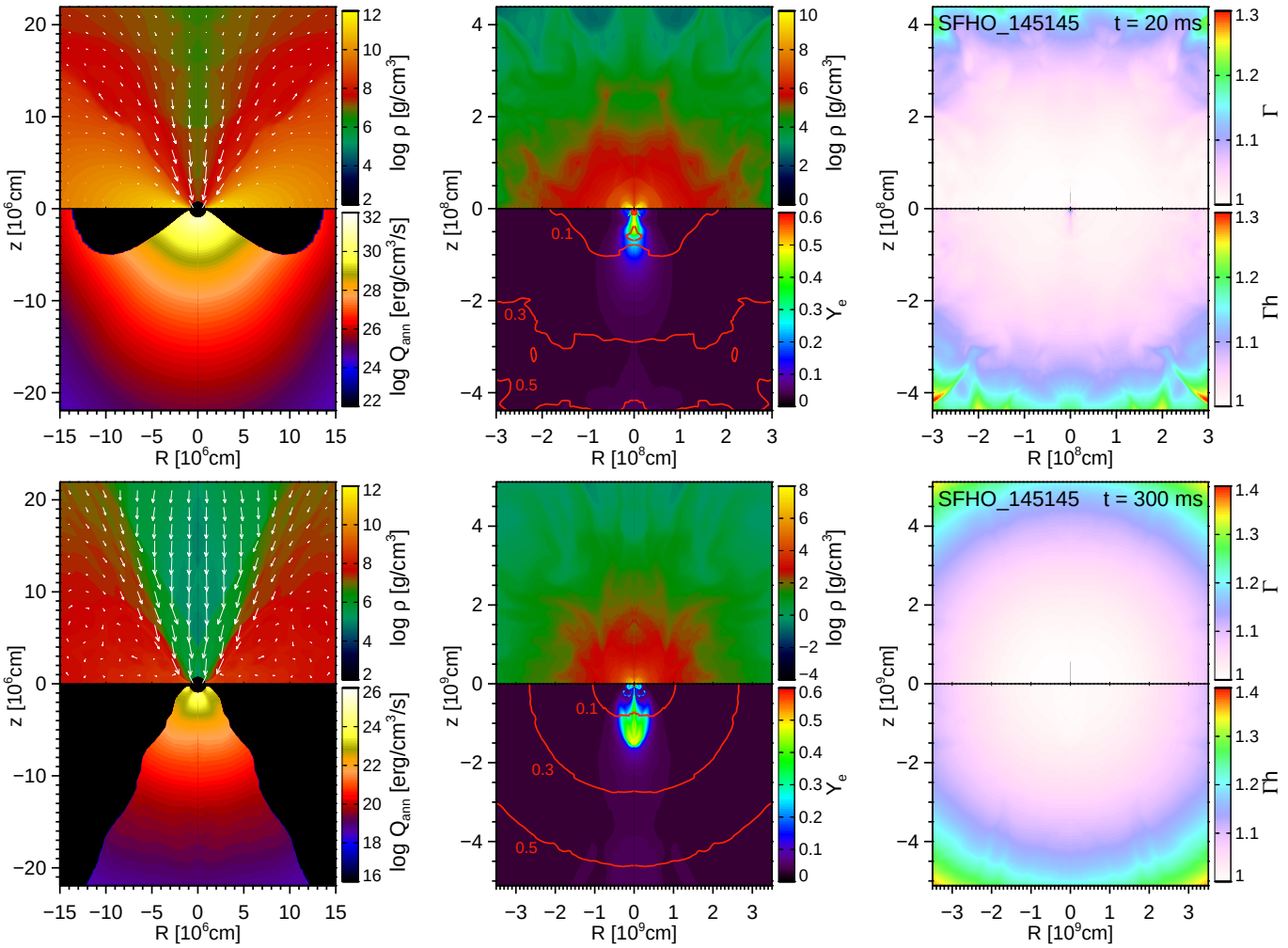

FIG. 2.— Maps of density, ρ, annihilation rate, $Q_{\rm ann}$, electron fraction, Y_e, Lorentz factor, Γ, and terminal Lorentz factor, Γh, for NS-NS merger model SFHO_145145 at the two times indicated in the right panel of each row. Note the different spatial and color scales for different times. Arrows indicate the poloidal (i.e. projected into the R-z plane) velocity vectors. Their length is limited to the distance between two neighboring arrows, which corresponds to $0.2\,c$. The red lines are isocontours of the poloidal velocity at values labeled in units of c.

radius. The total annihilation rate, $\dot{E}^{\rm pol}_{\rm ann} \equiv \int_{V,45} Q_{\rm ann} {\rm d}V$ (with the integral performed only in the two polar cones with 45° half-opening angle), is roughly proportional to $L_{\nu_e} L_{\bar{\nu}_e}$, multiplied by additional factors accounting for the geometry of the emitting region and the preference for high neutrino mean energies $\langle\varepsilon\rangle_\nu$ (see, e.g., Goodman et al. 1987; Setiawan et al. 2006). The annihilation efficiency, $\eta_{\rm ann} \equiv \dot{E}^{\rm pol}_{\rm ann}/(L_{\nu_e} + L_{\bar{\nu}_e})$, is therefore approximately proportional to L_{ν_e} (noting that $L_{\bar{\nu}_e} \sim L_{\nu_e}$). Because L_ν decreases roughly like $\dot{M}_{\rm BH}$ (Fig. 1), $\eta_{\rm ann}$ declines earlier than η_ν and, hence, the time $T^{90}_{\rm ann}$, at which 90 % of the final $E^{\rm pol}_{\rm ann}$ has been deposited, is significantly shorter than the duration of the NDAF phase, $T_{\rm NDAF}$, defined as the time when η_ν drops below $\simeq 1$ % (Table 1).

The comparison between the models is facilitated by considering (Table 1) the global versions of the aforementioned efficiencies, $\bar{\eta}_\nu \equiv E_\nu/(m_{\rm torus}c^2)$ and $\bar{\eta}_{\rm ann} \equiv E^{\rm pol}_{\rm ann}/E_\nu$ with $E_\nu \equiv \int (L_{\nu_e} + L_{\bar{\nu}_e}){\rm d}t$, by which means the total annihilation energy $E^{\rm pol}_{\rm ann} = \bar{\eta}_\nu\,\bar{\eta}_{\rm ann}\,m_{\rm torus}c^2$. The emission efficiency, $\bar{\eta}_\nu$, is similar for all models (up to some reduction for higher viscosity caused by enhanced neutrino trapping at very early times). The main reason for this similarity are the comparable values of the dimensionless BH spin, $A_{\rm BH}$, for all models, which determine the amount of specific gravitational energy that can be released by gas before being accreted. Since approximately $\eta_{\rm ann} \propto L_\nu \propto \dot{M}_{\rm BH}$ we infer that $\bar{\eta}_{\rm ann}$ should grow for higher values of $m_{\rm torus}$ and $\alpha_{\rm vis}$, and a lower value of $M_{\rm BH}$. This turns out to be broadly consistent with our results. In the NS-BH model the positive effect of the high torus mass is more than counterbalanced by the reduced neutrino mean energies, $\langle\varepsilon\rangle_\nu$, compared to the NS-NS models (Fig. 1) and by the high BH mass, which leads to a longer accretion timescale.

Finally, the upper limit of energy available for any potential jet, represented by $E^{\rm pol}_{\rm ann}$, is given by $\sim (10^{-5}$–$10^{-4}) \times m_{\rm torus}c^2 \sim (1-2)\times 10^{49}$ erg in our models. The corresponding isotropic equivalent energies are almost independent of the polar angle (because of the approximate isotropy of the annihilation rates, see Figs. 2– 4) with $E^{\rm iso}_{\rm ann} \approx E^{\rm pol}_{\rm ann}/(1-\cos 45°) \sim (3-8)\times 10^{49}$ erg (Table 1).

3.2. *Polar outflows and ejecta interaction*

If and how much of $E^{\rm pol}_{\rm ann}$ can finally end up in an ultrarelativistic outflow depends crucially on the distribution of matter surrounding the torus. This is illustrated in Figs. 2– 4 for three representative models, of which each exhibits a qualitatively different outflow evolution.

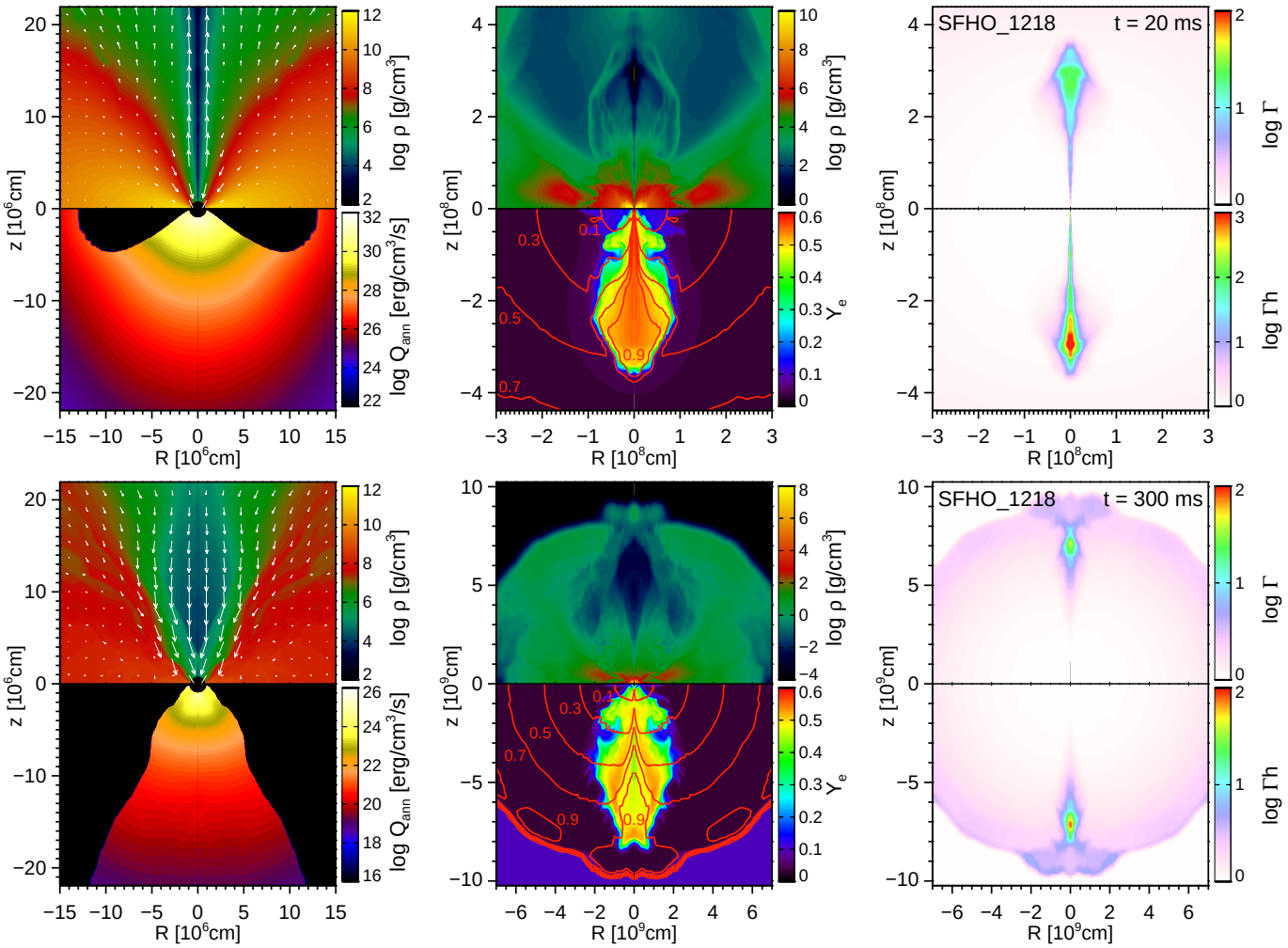

FIG. 3.— Same as Fig. 2 but for model SFHO_1218 and with partially different spatial and color scales.

In model SFHO_145145 (Fig. 2) the amount of baryonic pollution near the symmetry axis is so high that neutrino irradiation has hardly any impact, besides slightly accelerating the already expanding dynamical ejecta and raising their electron fraction, Y_e. The high densities are too prohibitive for annihilation to form a baryon-poor funnel, which is ultimately needed to produce high Lorentz factors.

In models SFHO_1218 (Fig. 3) and TM1_13520 the configuration is better suited for the development of relativistic outflows because the poles are loaded with relatively small amounts of matter. Hence, in both models funnels are successfully created, allowing jets to form and to expand outwards along the axis. Similar to jets in collapsars (e.g. MacFadyen & Woosley 1999; Bromberg et al. 2011), the jets consist of thin, ultrarelativistic beams surrounded by cocoons and mildly relativistically propagating heads. Right after the jets are launched, essentially all annihilation energy dumped into the funnels is used to power the beams, immediately increasing Γh (where Γ and h are Lorentz factor and specific enthalpy, respectively), which for adiabatic expansion represents an estimate for the terminal Lorentz factor. Therefore, the energy carried by material with $\Gamma h > 10$ and 100, $E_{\Gamma h>10/100}$, rises. The subsequent expansion of beam material then allows thermal energy to be converted into kinetic energy, leading to a growth also of $E_{\Gamma>10/100}$, the energy of material with $\Gamma > 10/100$ (see Fig. 1 for the time evolution of $E_{\Gamma h>10/100}$, $E_{\Gamma>10/100}$). However, the beam cannot expand freely as long as the jet is enveloped by dynamical ejecta. Hence, while being fed with annihilation energy at its base, the jet continually loses energy by drilling through the envelope. This happens at the expense of beam energy, which is transported to and dissipated at the much more slowly moving head. Once dissipated, this part of the energy is advected into the cocoon and is ultimately lost as potential contribution to a relativistic outflow. That is, only the fraction of original annihilation energy that is induced into the beam shortly before and after the time of an eventual break-out from the envelope could possibly be released within a relativistic outflow. However, in the considered NS-NS merger models the jet is not energetic enough to break out, which is why $E_{\Gamma h>10/100}$ successively decreases and finally vanishes (Figs. 1, 3).

Model TM1_1451, associated with a NS-BH merger, offers the most optimistic configuration for relativistic outflows, because the polar regions are essentially free of dynamical ejecta. However, neutrino-driven winds and the expansion of torus matter by viscous or other effects could still prohibit or impair the emergence of relativistic ejecta. Nevertheless, model TM1_1451 develops a powerful relativistic wind that contains 61 % (48 %) of the original annihilation energy in the form of $E_{\Gamma h>10}$ ($E_{\Gamma h>100}$), as measured at $t = 0.1$ s (Fig. 1). The radius-dependent half-opening angle of the outflow, θ, reflects the temporal change of the torus configuration (Fig. 4):

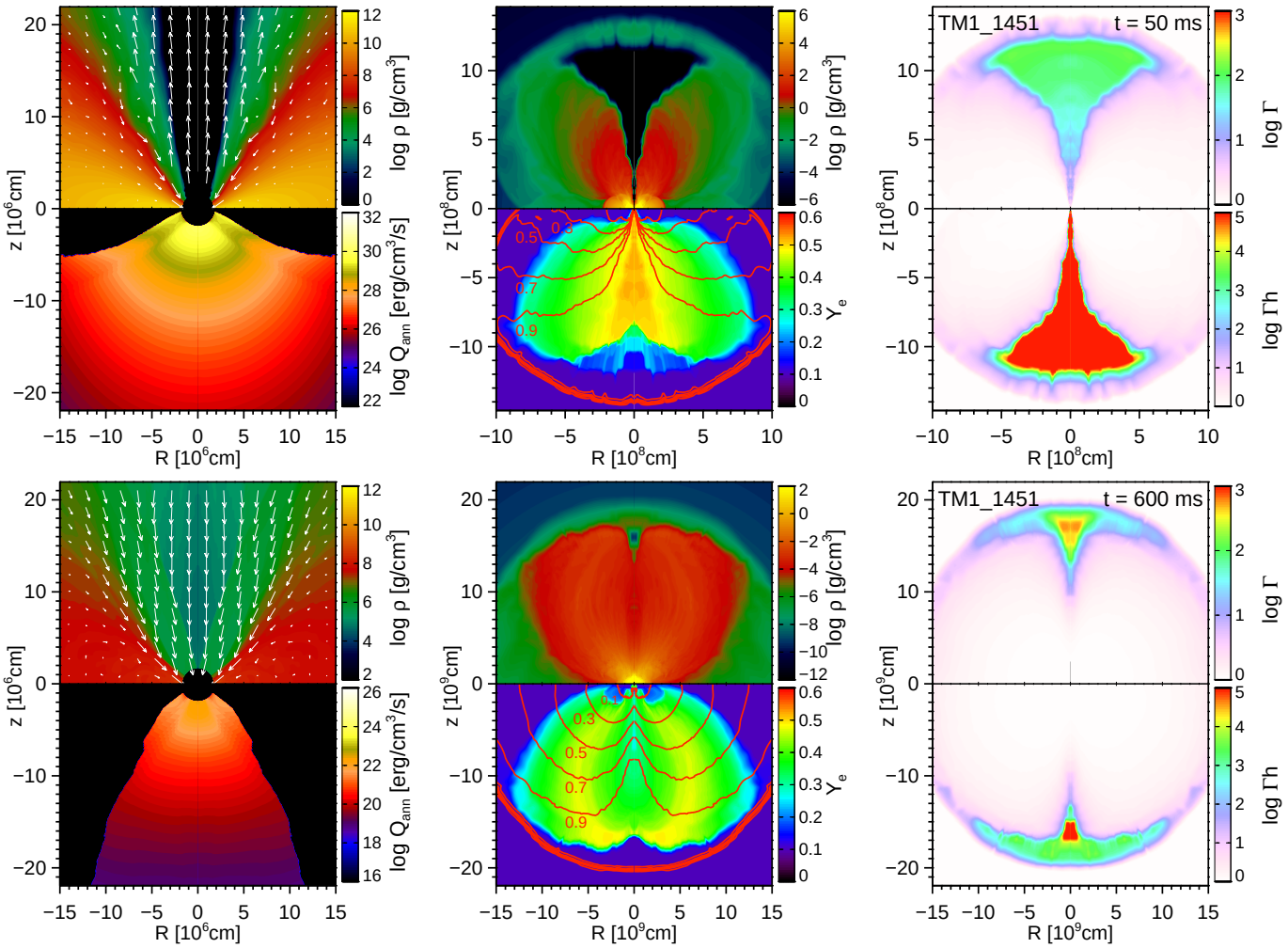

FIG. 4.— Same as Fig. 2 but for NS-BH merger model TM1_1451 and with partially different spatial and color scales.

At early times the torus is rather compact and can barely collimate the outflow, while subsequently the outer torus layers undergo viscous and neutrino-driven expansion and form a funnel, of which the walls collimate the outflow. Hence, the outflow consists of an ultrarelativistic ($\Gamma > 100$) core surrounded by less relativistic ($10 < \Gamma < 100$) wings (see Table 1 for the corresponding energies and half-opening angles). Interestingly, the collimation leads to a remarkable enhancement of the isotropic-equivalent energy of the ultrarelativistic core, $E^{\rm iso}_{\Gamma>100} \approx 2 \times 10^{50}$ erg, compared to that of annihilation, $E^{\rm iso}_{\rm ann} \approx 5 \times 10^{49}$ erg.

The distribution of Γ and the opening angles can still change somewhat after the final simulation time of $t = 0.6$ s because of a sizable fraction of the energy still residing in internal energy. However, the coarser grid at higher radii renders the late evolution more prone to numerical diffusion, which is why $E_{\Gamma>100}$ decreases at late times and we stopped the simulation.

3.3. *Conclusions*

We investigated the ability of $\nu\bar{\nu}$-annihilation to represent the dominant agent for generating sGRB viable outflows. In contrast to previous studies, which either computed the annihilation rates on a stationary background without any hydrodynamic feedback (e.g. Setiawan et al. 2006; Birkl et al. 2007; Richers et al. 2015) or which launched the outflow artificially (e.g. Aloy et al. 2005; Nagakura et al. 2014; Duffell et al. 2015), we self-consistently followed the combined neutrino-hydrodynamic evolution of the BH-torus system, the eventual launch of the jet in response to heating by $\nu\bar{\nu}$-annihilation, and the jet propagation through the envelope of dynamical ejecta produced during the binary merger. Our examined set of models covers the most relevant NS-NS and NS-BH configurations in the sense that they are both promising regarding the annihilation mechanism but still realistic enough to be abundantly present in nature.

We find that the total energy provided by annihilation, $E^{\rm pol}_{\rm ann}$, amounts to a fraction of about 10^{-5}–10^{-4} of the original torus rest-mass energy. Although this fraction grows with torus mass and viscosity, and for lower BH mass, we find typical values of $E^{\rm pol}_{\rm ann}$ not exceeding a few 10^{49} erg.

In the NS-BH merger remnant, which is essentially free of polar dynamical ejecta, annihilation heating is efficiently translated into a relativistic outflow, whose ultrarelativistic ($\Gamma > 100$) core is dynamically collimated to a half-opening angle $\theta_{\Gamma>100} \approx 8^\circ$ and an isotropic-equivalent energy $E^{\rm iso}_{\Gamma>100} \approx 2 \times 10^{50}$ erg. However, compared to the median values of observed sGRBs ($E^{\rm iso}_{\rm obs} \approx 2 \times 10^{51}$ erg and $\theta_{\rm obs} \approx 16 \pm 10^\circ$, see Fong et al. 2015), our results suggest that the annihilation mechanism is energetically too inefficient to explain the majority of sGRBs, but still could account for some low-luminosity events. This conclusion is further supported by

our result that the effective time of source activity obtained for our models is $T^{90}_{\rm ann} \lesssim 0.1$ s and thus much shorter than most observed times T^{90} of sGRBs (Fong et al. 2015). A lower viscosity or higher BH spin could possibly alleviate but not solve this issue.

Moreover, our simulations suggest that the $\nu\bar{\nu}$-annihilation energies in NS-NS mergers are too low to launch jets energetically enough to pierce through the envelope of dynamical ejecta, even in the most optimistic case of prompt BH formation and very asymmetric progenitors, which results in less baryon-polluted polar regions. If sGRBs are connected with NS-NS mergers, our results indicate that some other, probably magnetohydrodynamic processes (e.g. Paschalidis et al. 2015; Kiuchi et al. 2015; Dionysopoulou et al. 2015) are necessary at least to create and support a baryon-poor funnel through which the outflow can propagate without major dissipation. Once a funnel is established, however, $\nu\bar{\nu}$-annihilation could still play a non-negligible role in powering the outflow. Although we consider only NS-NS systems here where the MNS collapses rather early, our conclusions probably also hold for longer delay times. Then an even greater envelope mass would have to be penetrated by the jet because of the additional neutrino- and magnetically driven outflows from the MNS (Perego et al. 2014; Siegel et al. 2014).

We finally point out that several simplifications entered this study, e.g. the omission of accurate general relativistic effects, the use of viscosity to mimic magnetohydrodynamic turbulence, initial models that were not fully consistent with the merger remnants, and the remaining approximations of the neutrino transport.

OJ is grateful to Omer Bromberg for helpful discussions. We acknowledge support by the Max-Planck/Princeton Center for Plasma Physics (MPPC), by the DFG-funded Cluster of Excellence EXC 153 “Origin and Structure of the Universe”, by the European Research Council through grant CAMAP-259276, and by the Spanish Ministerio de Ciencia e Innovación through grant AYA2013-40979-P Astrofísica Relativista Computacional. The computations were performed at the Max-Planck Computing and Data Facility (MPCDF).

REFERENCES

Aloy, M. A., Janka, H., & Müller, E. 2005, A&A, 436, 273
Artemova, I. V., Bjoernsson, G., & Novikov, I. D. 1996, ApJ, 461, 565
Bauswein, A., Goriely, S., & Janka, H.-T. 2013, ApJ, 773, 78
Bauswein, A. O. 2010, PhD Thesis, Technische Universität München, München
Berger, E. 2014, ARA&A, 52, 43
Birkl, R., Aloy, M. A., Janka, H.-T., & Müller, E. 2007, A&A, 463, 51
Blandford, R. D. & Znajek, R. L. 1977, MNRAS, 179, 433
Bromberg, O., Nakar, E., Piran, T., & Sari, R. 2011, ApJ, 740, 100
Bruenn, S. W. 1985, ApJS, 58, 771
Chen, W. & Beloborodov, A. M. 2007, ApJ, 657, 383
Dessart, L., Ott, C. D., Burrows, A., Rosswog, S., & Livne, E. 2009, ApJ, 690, 1681
Di Matteo, T., Perna, R., & Narayan, R. 2002, ApJ, 579, 706
Dionysopoulou, K., Alic, D., & Rezzolla, L. 2015, Phys. Rev. D, 92, 084064
Dominik, M., Belczynski, K., Fryer, C., Holz, D. E., Berti, E., Bulik, T., Mandel, I., & O’Shaughnessy, R. 2012, ApJ, 759, 52
Duffell, P. C., Quataert, E., & MacFadyen, A. I. 2015, ApJ, 813, 64
Eichler, D., Livio, M., Piran, T., & Schramm, D. N. 1989, Nature, 340, 126
Fernández, R. & Metzger, B. D. 2013, MNRAS, 435, 502
Fong, W.-F., Berger, E., Margutti, R., & Zauderer, B. A. 2015, eprint arXiv:1509.02922
Foucart, F., O’Connor, E., Roberts, L., Duez, M. D., Haas, R., Kidder, L. E., Ott, C. D., Pfeiffer, H. P., Scheel, M. A., & Szilagyi, B. 2015, Phys. Rev. D, 91, 124021
Goodman, J., Dar, A., & Nussinov, S. 1987, ApJ, 314, L7
Hempel, M., Fischer, T., Schaffner-Bielich, J., & Liebendörfer, M. 2012, ApJ, 748, 70
Jaroszynski, M. 1993, Acta Astronomica, 43, 183
Just, O., Bauswein, A., Pulpillo, R. A., Goriely, S., & Janka, H.-T. 2015a, MNRAS, 448, 541
Just, O., Obergaulinger, M., & Janka, H.-T. 2015b, MNRAS, 453, 3386
Kiuchi, K., Sekiguchi, Y., Kyutoku, K., Shibata, M., Taniguchi, K., & Wada, T. 2015, Phys. Rev. D, 92, 064034
Kyutoku, K., Ioka, K., Okawa, H., Shibata, M., & Taniguchi, K. 2015, Phys. Rev. D, 92, 044028
Lattimer, J. M. 2012, Annual Review of Nuclear and Particle Science, 62, 485
MacFadyen, A. I. & Woosley, S. E. 1999, ApJ, 524, 262
McKinney, J. C. & Blandford, R. D. 2009, MNRAS, 394, L126
Metzger, B. D., Piro, A. L., & Quataert, E. 2008, MNRAS, 390, 781
Murguia-Berthier, A., Montes, G., Ramirez-Ruiz, E., De Colle, F., & Lee, W. H. 2014, ApJ, 788, L8
Nagakura, H., Hotokezaka, K., Sekiguchi, Y., Shibata, M., & Ioka, K. 2014, ApJ, 784, L28
Nakar, E. 2007, Phys. Rep., 442, 166
Oechslin, R., Rosswog, S., & Thielemann, F.-K. 2002, Phys. Rev. D, 65, 103005
Paczynski, B. 1986, ApJ, 308, L43
Paschalidis, V., Ruiz, M., & Shapiro, S. L. 2015, ApJ, 806, L14
Perego, A., Rosswog, S., Cabezón, R. M., Korobkin, O., Käppeli, R., Arcones, A., & Liebendörfer, M. 2014, MNRAS, 443, 3134
Piran, T. 2004, Reviews of Modern Physics, 76, 1143
Popham, R., Woosley, S. E., & Fryer, C. 1999, ApJ, 518, 356
Richers, S., Kasen, D., O’Connor, E., Fernández, R., & Ott, C. D. 2015, ApJ, 813, 38
Ruffert, M. & Janka, H.-T. 1999, A&A, 344, 573
Setiawan, S., Ruffert, M., & Janka, H.-T. 2004, MNRAS, 352, 753
—. 2006, A&A, 458, 553
Shakura, N. I. & Sunyaev, R. A. 1973, A&A, 24, 337
Siegel, D. M., Ciolfi, R., & Rezzolla, L. 2014, ApJ, 785, L6
Steiner, A. W., Hempel, M., & Fischer, T. 2013, ApJ, 774, 17
Usov, V. V. 1992, Nature, 357, 472
Woosley, S. E. 1993, ApJ, 405, 273
Zalamea, I. & Beloborodov, A. M. 2011, MNRAS, 410, 2302